Biochimica et Biophysica Acta 1837 (2014) 85–97

Contents lists available at ScienceDirect

Biochimica et Biophysica Acta

journal homepage: www.elsevier.com/locate/bbabio

Evidence for water-mediated triplet–triplet energy transfer in the photoprotective site of the peridinin–chlorophyll *a*–protein

Marilena Di Valentin *, Claudia E. Tait [1], Enrico Salvadori [2], Laura Orian, Antonino Polimeno, Donatella Carbonera

Dipartimento di Scienze Chimiche, Università di Padova, via Marzolo 1, 35131 Padova, Italy

ARTICLE INFO

Article history:
Received 28 May 2013
Received in revised form 5 July 2013
Accepted 10 July 2013
Available online 18 July 2013

Keywords:
Photoprotection
Light-harvesting
Pulsed EPR
ESEEM
QM–MM calculation
Hybrid DFT calculation

ABSTRACT

Experimental and theoretical studies indicate that water molecules between redox partners can significantly affect their electron-transfer and possibly also the triplet–triplet energy transfer (TTET) properties when in the vicinity of chromophores. In the present work, the interaction of an intervening water molecule with the peridinin triplet state in the peridinin–chlorophyll *a*–protein (PCP) from *Amphidinium carterae* is studied by using orientation selective ^{2}H electron spin echo envelope modulation (ESEEM) spectroscopy, in conjunction with quantum mechanical calculations. This water molecule is located at the interface between the chlorophyll and peridinin pigments involved in the photoprotection mechanism (Chl601(602)–Per614(624), for nomenclature see reference [1]), based on TTET. The characteristic deuterium modulation pattern is observed in the electron spin-echo envelopes for the PCP complex exchanged against ^2H_2O. Simulations of the time- and frequency-domain two-pulse and three-pulse ESEEM require two types of coupled ^{2}H. The more strongly coupled ^{2}H has an isotropic coupling constant (a_{iso}) of −0.4 MHz. This Fermi contact contribution for one of the two water protons and the precise geometry of the water molecule at the interface between the chlorophyll and peridinin pigments, resulting from the analysis, provide experimental evidence for direct involvement of this structured water molecule in the mechanism of TTET. The PCP antenna, characterised by a unity efficiency of the process, represents a model for future investigations on protein- and solvent-mediated TTET in the field of natural/artificial photosynthesis.

1. Introduction

Important electron transfer and energy transfer processes, including photoprotection via triplet–triplet energy transfer (TTET), occur in natural photosynthesis and provide the basis for the energy conversion process [2]. They have been widely studied in a variety of protein complexes, as well as in biomimetic systems. Mimicking nature by constructing artificial photosynthetic systems is an important research area where a detailed understanding of electron/energy transfer processes is invaluable [3–5]. The magnitude of the electronic coupling that governs the transfer reactions depends on several relevant factors, i.e., the electronic structure and the energies of the donor and acceptor groups, as well as the distance and orientation between them. Among these factors, the electronic structure and geometry of the intervening medium between the partners involved in the transfer must also be considered. In proteins, the surrounding residues and bridging molecules, including water, provide important pathways to finely optimise the electron/energy transfer efficiency [6].

Water enjoys a unique position as a medium for electron transfer. It can affect electron transfer rates by means of its electrostatic and quantum mechanical interactions with the redox partners. While several experimental and theoretical studies have focused on the efficiency of water in mediating electron-transfer processes in proteins and in bio-inspired supramolecular systems, with specific attention to its influence on the distance dependence of the electron transfer rates [7–13], only a small number of investigations have been carried out so far on solvent-mediated TTET [14–17].

The TTET process, based on Dexter's exchange mechanism [18], can be formalised as a simultaneous double electron transfer between the lowest unoccupied molecular orbitals (LUMOs) and the highest occupied molecular orbitals (HOMOs) and can be characterised by a non-adiabatic rate constant which depends on the exchange integral between the two electrons and thus on the electronic distribution over the molecular architecture involved in the process [19,20]. The overlap between wavefunctions may become critical at even shorter distances for TTET as compared to electron transfer. For this reason, superexchange models involving a bridge or the medium interposed between the donor and the acceptor molecules, which have been extensively discussed for electron transfer reactions [21], become even more important when describing TTET [22–27].

* Corresponding author. Tel.: +39 049 827 5139; fax: +39 049 827 5161.
E-mail address: marilena.divalentin@unipd.it (M. Di Valentin).
[1] Present address: Centre for Advanced Electron Spin Resonance, Department of Chemistry, University of Oxford, South Parks Road, Oxford OX1 3QR, UK.
[2] Present address: Institute of Structural and Molecular Biology and London Centre for Nanotechnology, University College London, Gower Street, London WC1E 6BT, UK.

0005-2728/$ – see front matter © 2013 Elsevier B.V. All rights reserved.
http://dx.doi.org/10.1016/j.bbabio.2013.07.005

The present paper is devoted to the spectroscopic characterisation of the TTET mechanism in the photosynthetic peridinin–chlorophyll *a*–protein (PCP), where the mechanism reaches unity efficiency [28] and an intervening water molecule between the partners involved in the transfer has been observed in the X-ray structure [1].

PCP is the peripheral water-soluble light-harvesting complex of most photosynthetic dinoflagellates, which constitute the main part of oceanic plankton. The PCP antenna complex of the dinoflagellate *Amphidinium carterae* can in many ways be considered as a model system for the study of energy transfer pathways in photosynthetic antenna complexes, due to its high symmetry, the availability of the X-ray structure at atomic resolution [1] and the high energy transfer efficiency [28]. A wealth of information not only on the singlet but also on the triplet transfer pathways in this complex is present in the literature [17,28–32].

The 2.0 Å X-ray structure reveals the presence of a non-crystallographic trimer of identical 32 kD subunits, each of which is constituted by a polypeptide forming a hydrophobic cavity containing the pigment molecules. The NH_2- and COOH-terminal domains of the monomer are characterised by a 56% sequence homology; each domain forms eight α-helices which bind a cluster of one chlorophyll *a* and four peridinin molecules (see Fig. 1A). The two domains are related by a pseudo-twofold symmetry axis, hence the two pigment clusters can be considered equivalent.

The PCP antenna is unique on account of the preponderance of carotenoid molecules, while in other light-harvesting complexes the chlorophylls predominate. The carotenoids in PCP are peridinins, highly substituted carotenoids, whose key structural features are a lactone and an allene group conjugated to the polyene chain, conferring special spectroscopic properties to the molecule [30]. The 4:1 ratio of peridinins to chlorophyll in PCP is explained by the necessity for efficient absorption of light in the blue-green region, which prevails in the marine habitat of dinoflagellates.

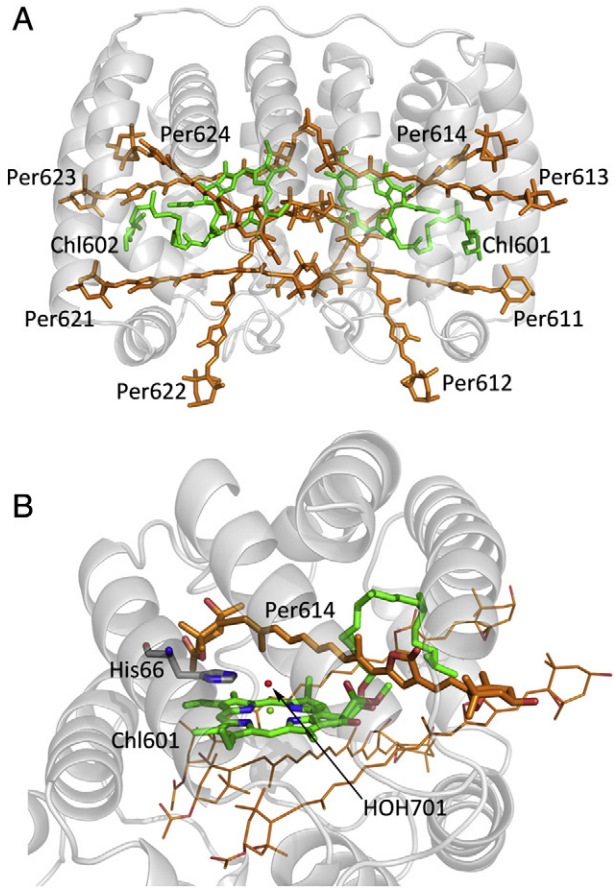

Fig. 1. (A) Pigment cluster associated with the basic unit of the PCP complex from *A. carterae* (PDB entry 1PPR)[1]; (B) Highlight of the molecules of the photoprotective site in the NH_2-terminal domain of PCP: peridinin 614, chlorophyll 601, the water molecule HOH701 coordinated to chlorophyll 601 and hydrogen-bonded to the histidine residue His66.

In addition to the light-harvesting function, peridinins fulfil the important function of protecting the system against photo-oxidative damage by quenching chlorophyll triplet states, formed under excess light conditions. Chlorophyll triplets sensitise the formation of singlet oxygen, which is a powerful oxidising agent capable of damaging the whole photosynthetic apparatus. By virtue of their low-lying triplet state, carotenoids are able to quench the chlorophyll triplet state as well as the singlet oxygen directly if it is formed.

Stringent structural conditions must be realised in the light-harvesting complex architecture in order to achieve high efficiency in the TTET process. In PCP, the chlorophyll molecules within each pigment cluster (Chl601 and Chl602) are arranged between two pairs of mutually orthogonal peridinins (Per611–Per612 and Per613–Per614 in the NH_2-terminal domain and Per621–Per622 and Per623–Per624 in the COOH terminus). The structure of PCP reveals two highly conserved histidine residues (His66 and His229), which are hydrogen-bonded to a water molecule (HOH701 and HOH678) acting as the fifth ligand of the chlorophyll's Mg ion. These water molecules are at the interface between Chl601 and Per614 and Chl602 and Per624, respectively, as highlighted for one of the two pseudo-symmetric couples in Fig. 1B. The identification numbers for amino acids, water molecules and pigments are in accordance with the X-ray nomenclature reported in reference [1].

The TTET in PCP has been extensively studied by means of advanced optical spectroscopies [28,31] and by Electron Paramagnetic Resonance magnetic (EPR) spectroscopies, exploiting the presence of the endogenous probe, the pigment triplet state [17,33–37]. Time-resolved EPR experiments, in conjunction with spectral simulations based on the theory of TTET, have allowed the identification of the specific path for triplet quenching [17]. It has been shown that the two pigment pairs Chl601–Per614 and Chl602–Per624, related by pseudo-symmetry, are responsible for photoprotection in the PCP antenna complex. The conclusion that the triplet state generated by TTET is localised on a single peridinin molecule, in each subcluster, is further supported by results of ENDOR (Electron Nuclear DOuble Resonance) experiments [33,35,36].

The identified peridinin molecule is distinguished by a smaller centre-to-centre distance to chlorophyll with respect to the other peridinin molecules of the pigment cluster, however all four peridinin molecules are at Van der Waals distance from the chlorophyll ring. The unique feature of the Chl601–Per614 (and equivalently Chl602–Per624) pair is the presence of the water molecule interposed between the two pigments (Fig. 1B) while no bridging molecules are present at the interface between the chlorophyll and the other peridinins. For this reason we raised the hypothesis that the interfacial water molecule might favour TTET by extending the overlap of the donor and acceptor wavefunction. This interfacial water molecule is also conserved in the high-salt PCP complex, a variant of the main form PCP, in the in vitro reconstituted PCP with different pigments and in the N89L-mutant, where the mutation of Asn-89 to Leu in the vicinity of Per614 has been introduced to study the effects of the environment on the spectroscopic properties. For all the variants this structural information is provided by high-resolution X-ray data [32].

In the present work, electron spin echo envelope modulation (ESEEM) spectroscopy is applied to yield information on small proton hyperfine couplings that could not be resolved in the ENDOR spectra of the peridinin triplet state. The aim is to characterise the structure of the photoprotection site in PCP and in particular to study the interaction between the interfacial water molecule and the carotenoid triplet state. This is achieved by combining ESEEM with hydrogen–deuterium exchange in order to highlight the exchangeable water protons in proximity to the paramagnetic centre. ^{2}H-ESEEM is experimentally convenient

and several studies have employed this method to assess interactions of exchangeable deuterons with paramagnetic centres, both in terms of hyperfine and quadrupolar tensors as well as number of coupled nuclei [38–52]. In systems where orientational selectivity is possible, both the principal values and the tensor orientations with respect to the structure can be assigned [53–55]. In the specific case of the photoexcited triplet state, it is possible to take advantage of orientation-selective ESEEM at the triplet state canonical field positions and derive the full set of hyperfine tensor components [56–58].

A detailed analysis of both two- and three-pulse ^{2}H-ESEEM data is undertaken to determine the number of exchangeable nuclei and the hyperfine interaction with the peridinin triplet state in a quantitative manner. The pulse EPR studies are combined with a quantum chemistry approach to identify the spatial arrangement of the interfacial water molecule, which is not defined in the X-ray structure, and to derive the hyperfine interaction tensors for the two protons of the water molecule. The derived spectroscopic parameters provide information on the electronic structure of the photoprotective site. The presence of a contact interaction between the electron spins of the peridinin triplet state and the nuclei of the water molecule unequivocally demonstrates that this water molecule, in addition to the chlorophyll and peridinin molecules, is an integral part of the photoprotective system in PCP, providing water-mediated electronic coupling.

2. Materials and methods

2.1. Sample preparation

PCP proteins, extracted and purified as described previously [59,60], were kindly supplied by R. G. Hiller. The sample concentration was ~1.4 mg/ml.

H/D exchange was achieved through dialysis with a deuterated buffer (50 mM tricine, 20 mM KCl, pD ~ 7.5) at 4 °C in N_2 atmosphere. A volume of about 1 ml of protein in protonated buffer was inserted into dialysis tubing (>12 kDa cut-off), which was then immerged into 40 ml of deuterated buffer. The deuterated buffer was exchanged twice. A part of the ^2H_2O-exchanged protein solution was removed after 1.5 h of dialysis and the rest was left in the deuterated buffer up to an overall exchange time of about 20 h.

2.2. Pulsed EPR measurements

Pulsed EPR experiments were performed on a Bruker Elexsys E580 EPR spectrometer operating at X-band and equipped with a dielectric ring resonator (EN4118X-MD4). The samples were excited with an Nd:YAG laser (Quantel Brilliant) at 532 nm with about 10 mJ per pulse and a repetition rate of 10 Hz. The measurements were performed at 20 K and the temperature was controlled with a helium cryostat (Oxford CF935) driven by a temperature controller (Oxford ITC503).

Field-swept echo-detected spectra were recorded using a 2-pulse (flash–DAF–π/2–τ–π–τ–echo) electron spin echo sequence for a delay after the laser flash (DAF) of 50 ns. The π/2 pulse was of 16 ns and the delay τ was set at 200 ns.

Two-pulse ESEEM experiments were performed with the two-pulse echo sequence flash–DAF–π/2–τ–π–τ–echo by incrementing τ. The initial delay time τ in the two-pulse experiments was chosen to be 100 ns and incremented in steps of 8 ns. The duration of the π/2 and π pulses was 16 and 32 ns respectively. The data set lengths were of 375 points.

Three-pulse ESEEM experiments were performed with the stimulated echo sequence flash–DAF–π/2–τ–π/2–T–π/2–τ–echo by incrementing T. The delay time τ was selected in order to maximise the deuterium contribution while suppressing that due to protons. The initial value of T was chosen to be 20 ns and varied in 12 ns increments. A total of 512 data points was recorded.

The ESEEM was measured at four different magnetic field positions, corresponding to the following zero field splitting (ZFS) canonical transitions of the peridinin triplet state: Z^- (300 mT), X^+ (328 mT), X^- (362 mT) and Y^- (375 mT) at 9.71 GHz. The measurements were performed with DAF of 50 ns or 13 μs between the laser pulse and the pulse sequence. Data were accumulated for 4–16 h, depending on the magnetic field position.

Two-step and four-step phase cycles were used for the two-pulse and three-pulse ESEEM, respectively. The final 10 points of each time domain data set were acquired with the integration window positioned 400 ns off the echo to define the background.

Details on the simulations of the echo-detected spectra can be found in the Supplementary information.

2.3. ESEEM data analysis

The ESEEM data were processed for analysis and interpretation both in the time and in the frequency domain. The data analysis was performed with a home-written program in MATLAB® following the ratio method proposed by Mims et al. [38]. The envelope obtained for the ^2H_2O-exchanged sample was divided by the envelope obtained for the untreated sample after normalisation of both envelopes. The quotient time trace was then dead-time reconstructed following a procedure proposed by Mims [61]. The dead-time reconstructed time traces were apodised with a Hamming window, zero-filled to 2048 data points and the spectra in the frequency domain were obtained by cosine Fourier transformation of the time-domain data.

2.4. Simulation of the ESEEM data

Simulations of both the time and frequency domain ESEEM data were performed with home-written programs in MATLAB® based on the *saffron* routine of *EasySpin* (version 3.1.7) which computes the modulation frequencies and the amplitudes of the corresponding peaks and constructs a spectrum histogram [62,63]. The time domain signal is obtained by inverse Fourier transform.

Orientation and transition selection in systems with anisotropic electron spin Hamiltonians, as in the case of triplet states, are accounted for by pre-computing the orientations contributing to the ESEEM spectrum for a certain microwave field and pulse excitation width based on the parameters of the spin Hamiltonian, e.g., the ZFS tensor in triplet state systems. The ESEEM signal is then computed only for these orientations and summed with the appropriate weights. The input parameters for the simulation are:

i) coefficients D and E, defining the ZFS interaction,
ii) principal values of the dipolar hyperfine interaction tensor A_{xx}, A_{yy} and A_{zz} and the isotropic hyperfine interaction constant a_{iso},
iii) $e^2qQ\hbar^{-1}$ and η defining the nuclear quadrupole interaction, and
iv) Euler angles defining the orientation of the interaction tensors with respect to the molecular frame.

The ZFS parameters D and E were taken from literature [33] and the orientation of the ZFS tensor was determined by principal component analysis [64], as described in detail in the Supplementary data.

Initial simulation parameters for the hyperfine interaction tensor for the hydrogen/deuterium atoms of the H0H701 molecule were obtained from DFT calculations (see below) and were optimised for the best agreement with experimental time- and frequency-domain data. The nuclear quadrupole interaction parameters of e^2qQ and η used were those reported in a nuclear quadrupole resonance study on isotopically enriched Ice II ($e^2qQ = 0.25$ MHz, $\eta = 0$)[65]. The principal axis of the nuclear quadrupole tensor of deuterium in deuterated water was assumed to be directed along the O–^{2}H bond and the Euler angles with respect to the molecular frame were calculated accordingly.

ESEEM simulations for the deuterons on the Per614 molecule were performed using the hyperfine values obtained from DFT calculations.

The contributions of matrix deuterons to the ESEEM traces were estimated by calculating the dipolar hyperfine interaction with the point-dipole approximation for a series of "test protons" at positions defined by a three-dimensional grid surrounding Per614 on the X-ray structure. Since the spin density in Per614 is distributed along the whole conjugated chain, the dipolar interaction has to be calculated as a weighted sum of point-dipolar interactions between the nucleus and the various atoms over which the spin density is distributed, i.e. $A_{total} = \sum_i \rho_i A_i$ where A_i is the dipolar tensor calculated for the interaction of the nucleus with the normalised spin density ρ_i on the atom i.

The dipolar hyperfine tensor components of the "test protons" located at each intersection point of the defined grid were evaluated and hyperfine isosurfaces based on the intermediate component of the hyperfine tensor, A_{mid}, were computed with a numerical method proposed in references [66,67]. The isosurfaces were used to evaluate the number of exchangeable protons at different distances from Per614 using the coordinates of the exchangeable protein backbone protons and free water molecules from the X-ray structure. Their contribution to the ESEEM traces was computed by assuming an axial hyperfine tensor with the principal values $[A_{mid}, A_{mid}, -2A_{mid}]$ for each isosurface and by summing the contributions of the different nuclei according to the product rule. The overall procedure was implemented in a home-written MATLAB® program.

2.5. Computational details

The geometry of the molecular cluster involved in the photoprotective mechanism in PCP was optimised at DFT [68–70] as well as ONIOM [71,72] level of theory as implemented in Gaussian [73]. Initially a DFT ground state optimisation with no constraints of a system constituted by Per614, Chl601 without phytol chain, the sidechain of His66 and the water molecule HOH701 coordinated to the Mg^{2+} ion of Chl601, according to X-ray nomenclature [1], was performed at B3LYP/6-31G(d) [74,75] level of theory; PBE0/6-31G(d) [76–78] was also tested and gave almost identical structural results. Both these levels of theory were previously tested in model systems and also in that case gave similar structural results [79]. The input coordinates were taken from the X-ray structure (PDB entry 1PPR) [1].

The structure obtained with full optimisation was not a satisfactory model of the photoprotective site due to the excessive curvature of the peridinin molecule, the variation of the relative orientation of the Per614–Chl601 pair and the rearrangement of the unconstrained histidine residue, moving away from the chlorophyll ring and changing the position of the hydrogen-bonded water molecule accordingly. Therefore, a series of constrained geometry optimisations, including additional residues, were performed. The best results, in terms of least displacement from the X-ray reference structure were obtained for the system constituted by Per614, Chl601 without phytol chain, the sidechain of His66, the water molecule HOH701 coordinated to the Mg^{2+} ion of Chl601 and five surrounding amino acids (His66, Gly78, Ile96, Glu101 and Gln150) kept frozen in the original crystallographic positions during the optimisation. This provided strong evidence in favour of the importance of the surrounding matrix and prompted us to perform ONIOM calculations, with the aim of obtaining a reliable geometry without imposing artificial constraints.

In an ONIOM B3LYP/6-31G(d):UFF full optimisation the higher (inner) layer, i.e., the same system used in the full geometry optimisation, was described at B3LYP/6-31G(d) level; the lower (outer) layer, treated at molecular mechanics level [80], was defined by including all the residues of the protein surroundings located at a distance of 4 Å from the atoms of the peridinin and the chlorophyll ring. This geometry is in very good agreement with the X-ray structure and has been used for subsequent calculations unless stated otherwise in the text.

The spin density of the triplet state was computed in vacuo at the B3LYP/6-311G(d,p) level of theory on the Chl601–Per614–HOH701 system extracted from the ONIOM optimised geometry. As the symmetry of Per614 and Per624 is conserved in terms of spin density distribution on the carotenoid triplet state [33], all calculations were performed considering the NH_2-terminal domain of the PCP complex from *A. carterae*. Spin contamination does not affect the resulting triplet wavefunction. The hyperfine coupling parameters of the H atoms of HOH701 were calculated with B3LYP and the purposely tailored EPRII basis set for H, C, N and O nuclei [81–83] and the 6-311G(d,p) basis set for Mg [84,85]. The EPRII basis set has proven to be generally accurate in EPR parameter calculations [86,87].

Environmental effects on the spin density and the hyperfine coupling parameters have been included by employing the Polarisable Continuum Method [88] with a dielectric constant of 3.0 (levels of theory PCM-B3LYP/6-311G(d,p) and PCM-B3LYP/EPRII-6-311G(d,p)) which is in the range estimated for light-harvesting proteins and previously employed in similar calculations [89–91].

3. Results

3.1. ESEEM experiments

In Fig. 2A the field-swept echo-detected EPR spectrum of the PCP complex of *A. carterae* recorded at 20 K and with a DAF of 50 ns is shown. An identical spectrum is obtained for the deuterated PCP complex. The canonical transitions are highlighted together with the ZFS axis directions with respect to the molecular frame. The EPR spectrum of the peridinin triplet state is significantly wider than the microwave pulse excitation bandwidth and hence orientation selection applies for pulse EPR experiments. ESEEM data were collected at four field positions, corresponding to the following canonical transitions of the triplet state: Z^-, Y^-, X^- and X^+.

The two-pulse echo and the three-pulse echo envelopes collected for the untreated and ^2H_2O-exchanged samples, at the field position corresponding to the high-field transition for spin systems with the ZFS axis X directed along the magnetic field direction, and the corresponding quotient envelopes are reported in Fig. 2B and C.

Both the two- and three-pulse echo traces collected for the untreated and ^2H_2O-exchanged samples show a high frequency modulation due to the hydrogen atoms coupled to the peridinin triplet state. The envelope of the ^2H_2O-exchanged sample shows additional modulations at a slower frequency, due to deuterium nuclei. The deuterium modulations are enhanced by the division of the envelopes of the ^2H_2O-exchanged and the untreated sample. The quotient traces resulting from the envelope division procedure are characterised by a shallow modulation pattern with a frequency close to the deuterium Larmor frequency, indicating the presence of super-hyperfine interactions. The marked attenuation of the modulations with time points to the fact that they are due to a small number of nuclei, since many weakly coupled nuclei would cause slow modulation damping [92].

The spin polarisation of the field-swept echo-detected EPR spectrum of peridinin is also reflected in the ESEEM time traces, which can be either emissive or absorptive, depending on the spin polarisation at the considered magnetic field position. For example for the X^+ transition the ESEEM envelopes are emissive, as shown in Fig. 2. The echo intensity, depending on the spin polarisation, varies greatly with the magnetic field position, thus influencing the signal-to-noise ratio of the corresponding ESEEM time trace. The echo has its maximum intensity at the X^- and X^+ field positions, while the echo intensity at the $Y^{+/-}$ field positions is so low as to prevent the ESEEM measurement with a DAF of 50 ns. However, kinetic studies of the triplet state evolution in PCP have shown that a spin polarisation inversion accompanied by an increase in signal intensity occurs for the Y transitions for increasing DAF intervals, due to the strongly anisotropic decay of the three triplet state spin sublevels [17]. This allows the detection of ESEEM at delay times corresponding to the maximum spin polarisation inversion.

The overall set of orientation-selective two-pulse and three-pulse quotient ESEEM traces for the canonical Z^-, Y^-, X^- and X^+ transitions are shown in Fig. 3 (left panels). While the quotient traces at the X^+, X^- and Y^- field positions show weak modulations due to coupled deuterium nuclei, those at the Z^- field position are still characterised by the presence of some modulations at the proton Larmor frequency, while no modulations at the deuterium Larmor frequency are visible. The magnetic dependence of the modulation frequency and amplitude is indicative of strong orientation selection.

In Fig. 3 (right panels) the cosine Fourier transforms of the time-domain data are also shown. The resulting two-pulse frequency spectra exhibit a positive peak around 2.0 MHz (ranging from 1.95 MHz for the Z^- to 2.5 MHz for the Y^- field position, with the X^+ and X^- positions at intermediate values of 2.2 and 2.3 MHz), corresponding to the ^2H Larmor frequency, and a ^2H sum combination peak at twice that frequency, which is marked by the opposite phase. The three-pulse frequency domain spectra present a prominent peak around 2.0 MHz, while no combination line, which would be indicative of the presence of multiple deuterium nuclei coupled to the unpaired electron spins [92], is visible. This result suggests that a limited number of nuclei are contributing to the ESEEM envelope. A signal with a derivative shape close to the proton Larmor frequency in some of the spectra is due to the incomplete elimination of the proton contribution by the envelope division procedure.

The rate of exchange can vary greatly for different protons in different environments in proteins. For this reason, the protein sample was exposed to ^2H_2O for two different times for a qualitative evaluation of the extent of $^1H/^2H$ exchange. The ESEEM time traces recorded for the samples with exchange times of 1.5 and 20 h are identical after division by the time trace of the untreated sample (Fig. S1, Supplementary data). The presence of a greater number of deuterons in the environment of the peridinin triplet state in the sample with the longer exchange time would cause an increase of the modulation depth, which however is not observed. It can thus be concluded that all the exchangeable protons in the environment of the paramagnetic species are exchanged within a short time; in the following only the 1.5 h-exchanged data are considered.

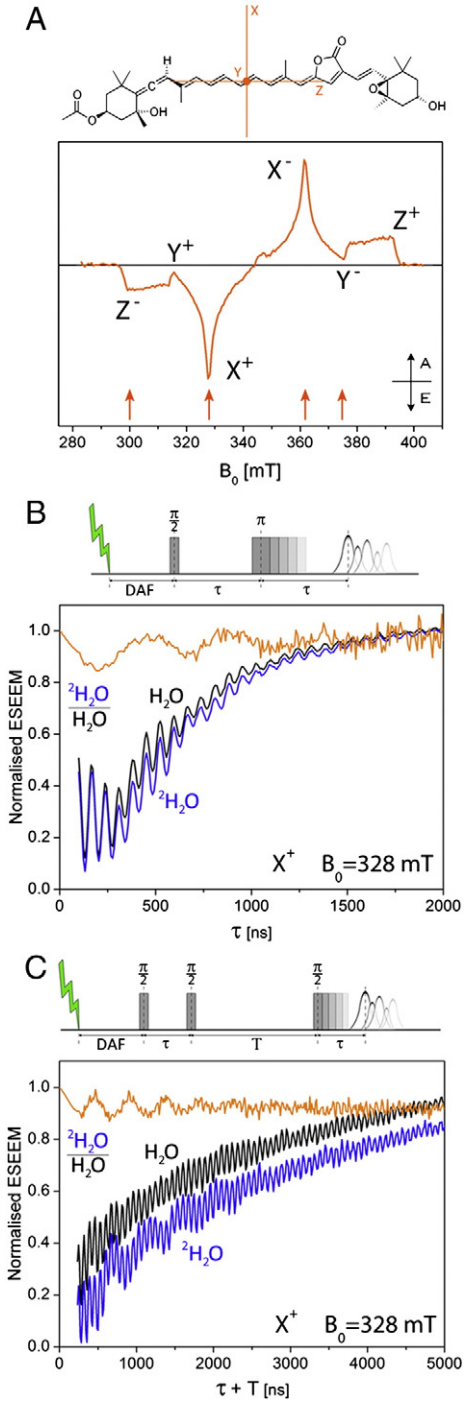

Fig. 2. (A) Field-swept echo-detected EPR spectrum of the peridinin triplet state in PCP from *A. carterae* at 20 K (ν_{mw} = 9.71 GHz). ZFS tensor canonical orientations are labelled in the spectrum. The arrows indicate the field positions at which the ESEEM experiments were performed. Spin polarisation: EAEAEA. (A = absorption, E = emission). The molecular structure of peridinin with the direction of the ZFS principal axes is shown above the spectrum. Two-pulse (B) and three-pulse (C) ESEEM time traces collected at the X^+ field position in water (black) and deuterated water (blue) and normalised dead-time reconstructed quotient traces obtained by envelope division as described in the text (orange). The ordinate scale refers only to the quotient ESEEM traces. The corresponding pulse sequences are shown above the graphs.

3.2. Computational results

Quantum mechanical calculations provide the optimised geometry of the region of interest in the protein employed for simulation and interpretation of the triplet state pulse-EPR data. The spin densities and hyperfine parameters are calculated for selected geometries and used for the simulation of the experimental ESEEM traces. Since magnetic spectroscopy parameters are highly sensitive to an accurate definition of the molecular structure, particular care was devoted to a careful determination of the system geometry. Our first attempts of fully optimising the molecules of the protein-pigment cluster, believed to constitute the photoprotective site in PCP, led to severely distorted geometries at B3LYP/6-31G(d) as well as at PBE1PBE/6-31G(d) level of theory. In these calculations, the photoprotective site included the peridinin molecule (Per614), whose triplet state is detected in the EPR experiments as demonstrated in reference [17], the chlorophyll molecule (Chl601), its partner in the TTET, the water molecule (HOH701), which is interposed between these two molecules and the histidine residue (His66) hydrogen-bonded to the water molecule (see Fig. 4).

The agreement between the X-ray and computed structures improved considerably after introducing some ad hoc geometry constraints to the relative orientation of the pigments and by taking some selected residues of the protein environment into account as well; this was ascribed to the importance of the surrounding protein matrix in determining the conformation and relative orientation of the pigment molecules. Thus ONIOM calculations at B3LYP/6-31G(d):UFF level were performed with the aim of modelling the effect of the protein environment on the structure of the photoprotective site without imposing artificial constraints. In the ONIOM optimisation the outer layer was defined by residues with a distance of 4 Å from the atoms of Chl601 and Per614; the inner layer was formed by Chl601, Per614, HOH701 and His66.

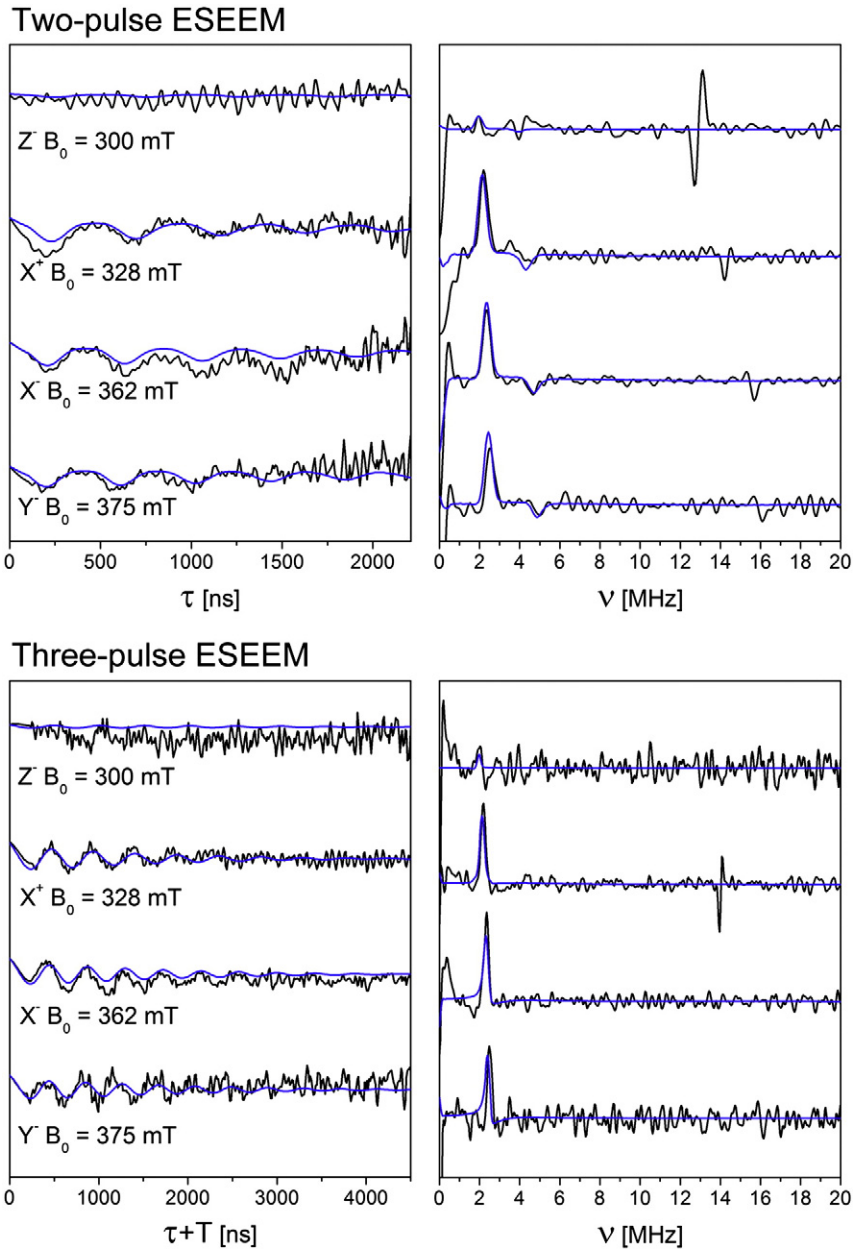

Fig. 3. Experimental two- and three-pulse ESEEM time traces and FFT spectra (black) of the peridinin triplet state in PCP at 20 K ($\nu_{mw} = 9.71$ GHz), compared to the corresponding simulations (blue) with the optimised hyperfine interaction parameters reported in Table 2.

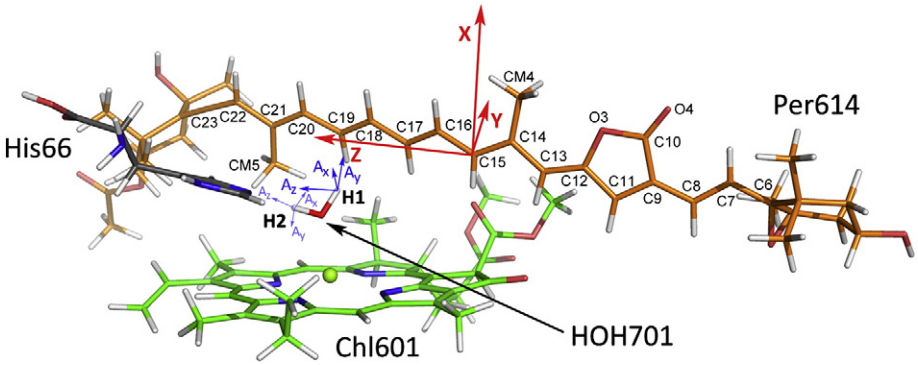

Fig. 4. Structure of the photoprotective site in PCP, consisting of Chl601, Per614, His66 and HOH701, as resulting from the B3LYP/6-31G(d):UFF geometry optimisation. The ZFS axes of peridinin are shown in red and the hyperfine interaction tensor axes of the two protons of the water molecule HOH701 resulting from the B3LYP/EPRII-6-311G(d,p) calculation are shown in blue.

The compatibility of the ONIOM optimised geometry with experimental field-swept echo-detected EPR spectra of the peridinin triplet state in the PCP antenna complex was tested by calculation of the triplet state EPR spectrum of Per614, on the basis of the optimised structure. In the framework of spin angular momentum conservation, the triplet state sublevel populations, determining the polarisation of the calculated spectrum, depend on the squared cosines of the angles between the Per614 and Chl601 ZFS axes. This method is thus highly sensitive to the relative orientation of the peridinin and chlorophyll molecules [17]. The calculated spectrum correctly reproduces the spin polarisation of the experimental echo-detected spectrum (see Fig. 5). The relative orientation of the peridinin and chlorophyll molecule in the optimised geometry is thus in satisfactory agreement with EPR data as well as the crystal structure coordinates [1]. In contrast, the calculated EPR spectra on the basis of the fully or constrained optimised structures at B3LYP/6-31G(d) level of theory only give a poor agreement with the experimental data (Fig. S2, Supplementary data).

It is worth noticing that in the optimised geometry the position and orientation of the water molecule HOH701 is imposed by the interactions with the surrounding molecules, i.e., chlorophyll, histidine and to a lesser extent peridinin. The determined Mg–O distance (2.1 Å) falls into the range of typical distances for water coordinated to porphyrin rings [93] and confirms coordination of the water molecule to the Mg ion of the chlorophyll molecule. The position of one water proton is fixed by hydrogen-bond formation with the histidine residue and the second hydrogen atom is found to point towards the conjugated chain of peridinin (details in Fig. S3, Supplementary data).

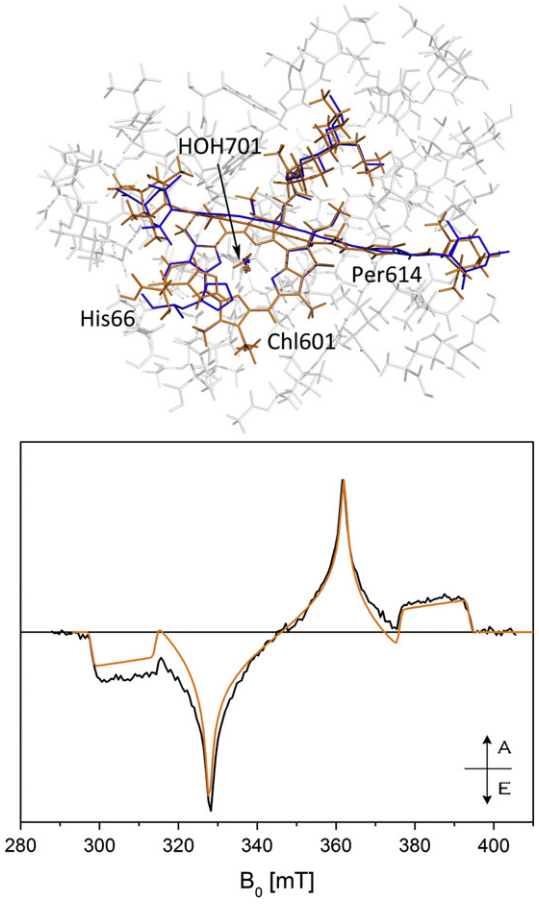

Fig. 5. Top: comparison between the X-ray structure and the B3LYP/6-31G(d):UFF optimised structure of the photoprotective site with superimposed chlorophyll rings: Chl601, Per614, His66 and HOH701are shown in blue (X-ray) and orange (ONIOM). Bottom: comparison of the experimental field-swept echo-detected EPR spectrum of the peridinin triplet in the PCP complex at 20 K (black) and the EPR spectrum calculated for the arrangement of the Chl601/Per614 pair in the optimised structure (orange). (A = absorption, E = emission).

Computations of triplet spin density were carried out on the Chl601–Per614–HOH701 system extracted from the geometry optimised at B3LYP/6-31G(d):UFF level and led to the identification of a low-lying triplet state localised on the peridinin moiety. The corresponding spin densities on the carotenoid molecular skeleton and on the water molecule are reported in Table 1 (for atom positions see Fig. 4). The same calculation was performed by embedding the molecular cluster in a dielectric medium ($\varepsilon = 3.0$) and the corresponding spin densities are also reported in Table 1. The result is in accordance with previous calculations on the isolated peridinin triplet state [33,36]. However, the extension of the system to the water molecule at the interface between the Per614 and Chl601 pair allows a more detailed mapping of the spin density: a small but significant spin density on the oxygen atom of HOH701 was found.

The hyperfine coupling parameters for the hydrogen atoms of the water molecule were calculated at B3LYP/EPR-II-6-311G(d,p) level of theory on the chlorophyll–peridinin–water complex (Chl601–Per614–HOH701) extracted from the ONIOM optimised system. The computed hyperfine interaction tensors for the two protons of the water molecule, containing both the isotropic and dipolar contributions, are reported in Table 2; the corresponding deuterium hyperfine couplings can be derived through multiplication by the ratio of nuclear g values ($g_n(^2H) / g_n(^1H) = 0.1535$). The orientation of the hyperfine interaction tensor, described in Table 2 in terms of Euler angles with respect to the ZFS tensor, is depicted in Fig. 4.

An inspection of the hyperfine interaction parameters for the two water protons shows that the water proton closer to the conjugated chain of peridinin (H1 in Fig. 4) is more strongly coupled to the peridinin triplet state and characterised by a significant isotropic hyperfine interaction constant ($a_{iso} = -0.4$ MHz) while the isotropic contribution becomes almost negligible for the more distant proton (H2).

3.3. ESEEM data analysis

Detailed information on the isotropic and anisotropic hyperfine parameters of the deuterons interacting with the peridinin triplet

Table 1
Mulliken spin densities of selected atoms on the system constituted by the conjugated chain of Per614 and the water molecule HOH701.

Atom[a]	B3LYP/ 6-311G(d,p)[b]	PCM-B3LYP/ 6-311G(d,p)[b]
C6	−0.017	−0.017
C7	0.202	0.198
C8	−0.093	−0.091
C9	0.242	0.234
C10	0.016	0.028
C11	−0.048	−0.031
C12	0.257	0.250
C13	0.011	0.019
C14	0.228	0.224
C15	0.191	0.191
C16	0.065	0.063
C17	0.300	0.299
C18	−0.076	−0.077
C19	0.334	0.331
C20	−0.131	−0.128
C21	0.300	0.298
C22	−0.099	−0.098
C23	0.208	0.207
C24	−0.038	−0.038
CM4	−0.015	−0.015
CM5	−0.022	−0.022
O4	0.135	0.130
O (H_2O)	0.002	0.002

[a] Atom numbering as shown in Fig. 4.
[b] For Per614 only spin densities larger than 0.015 (in absolute value) are included in this table.

Table 2
Hyperfine parameters for the two protons of the water molecule labelled as shown in Fig. 4.

	H1		H2	
	B3LYP/ EPRII-6-311G(d,p)	Simulation[a]	B3LYP/ EPRII-6-311G(d,p)	Simulation[a]
A_{xx} (MHz)	−1.9	−2.5	0.7	0.8
A_{yy} (MHz)	1.8	2.5	−0.6	−0.7
A_{zz} (MHz)	0.1	0.0	−0.1	−0.1
a_{iso} (MHz)	−0.4	−0.4	−0.1	−0.1
α (°)[b]	130	130	50	50
β (°)[b]	6	6	20	20
γ (°)[b]	−170	−170	20	20

[a] Error of ±0.2 MHz on the hyperfine parameters.
[b] Euler angles defining the orientation of the HFI tensor with respect to the ZFS tensor, errors of ±5° on β and of ±10° on α and γ.

state and on the number of contributing nuclei can be extracted from the experimental data by means of numerical simulations of the ESEEM spectra. Fig. 3 shows the simulations of the two- and three-pulse ESEEM traces in the time and frequency domain for all canonical transitions of the peridinin triplet state.

The time and frequency domain data of two- and three-pulse ESEEM are analysed in parallel, as some information can be extracted more easily by considering the time domain, other by considering the frequency domain. The analysis of the time domain data is particularly important in the case of weak hyperfine interaction, where the nuclear frequencies do not differ considerably from the Larmor frequency of the nucleus and the main information on the spin system can be derived from the modulation depth and the decay of the modulations [92].

All the exchanged protons in the surroundings of the peridinin molecule are expected to contribute to the modulation depth. The exchangeable protons in the environment of the photoprotective Per614 molecule can be divided into three classes:

(1) exchangeable protons of the protein structure, on the other pigment molecules of the protein complex or on exchangeable water molecules;
(2) exchangeable protons on the peridinin molecule Per614 itself;
(3) exchangeable protons of the water molecule (HOH701) at the interface between Per614 and Chl601.

The protons belonging to the first class are referred to in the following as exchangeable matrix protons. The contributions to the modulation depth of the different classes of exchangeable protons are hereafter discussed separately.

3.3.1. Matrix protons and exchangeable protons on the peridinin molecule

To evaluate whether or not the matrix contributions alone could explain the observed modulations, the exchangeable protons in the surroundings of Per614 were identified in the X-ray structure up to a distance of 15 Å, after the addition of the hydrogen atoms as described in the Materials and methods section, and considered in the simulation of the ESEEM time trace. Evaluation of the matrix contributions can be greatly simplified by employing the spherical model [92,94] which is, however, not realistic in the present case, given the elongated spin density distribution of the peridinin triplet state. For this reason the modulations were averaged for nuclei randomly distributed on hyperfine isosurfaces rather than on spheres. The dipolar hyperfine interaction isosurfaces were evaluated numerically (see Section 2.4), considering the middle-valued component of the hyperfine interaction tensor A_{mid} as the most significant in terms of its influence on the deuterium ESEEM patterns in analogy to other ESEEM studies [66,67]. The three-dimensional isosurfaces of A_{mid} are represented with respect to Per614 in Fig. 6A.

All the matrix protons contained on a specific isosurface, belonging to amino acid residues, to water molecules or to the other pigment molecules, were considered to give a contribution to the ESEEM determined by the hyperfine interaction value assigned to that isosurface. The corresponding echo envelope modulation was simulated assuming an axial hyperfine interaction with $A = A_{mid}$ and the contributions of the different nuclei were summed according to the product rule [92]. Most of the exchangeable protons identified in the environment of Per614 are positioned outside the 0.01 MHz isosurface and the

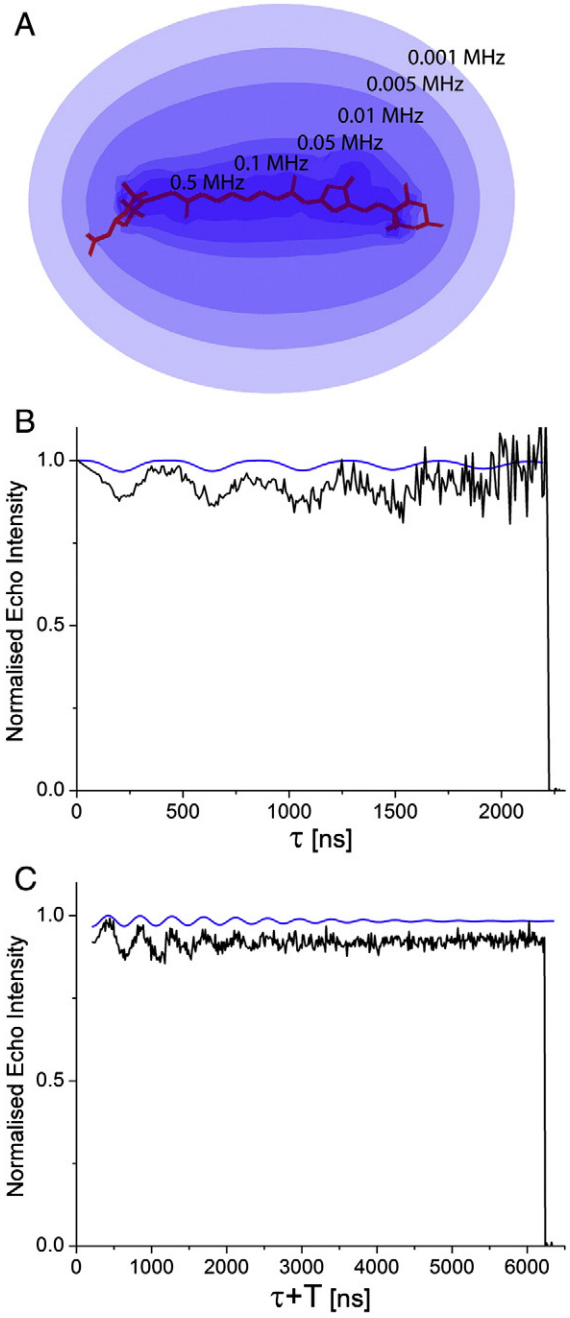

Fig. 6. (A) Hyperfine isosurfaces of the intermediate hyperfine interaction component for the exchangeable matrix protons in PCP with respect to Per614. Two- (B) and three-pulse (C) ESEEM traces calculated for matrix protons with the modified spherical model approximation explained in the Materials and methods section, assuming all exchangeable matrix protons in PCP to be substituted by deuterons. The simulated data are compared with the experimental echo envelopes recorded at the X^- field position (362 mT at ν_{mw} =9.71 GHz).

calculations have shown that the hyperfine tensor rhombicity would be small at these distances from Per614; hence the approximation introduced in assuming an axial hyperfine interaction is valid.

The ESEEM simulations of the two- and three pulse quotient ESEEM envelopes, resulting from this modified spherical model analysis, are reported in Fig. 6B and C respectively. The simulated modulation depths for the matrix proton contributions are far too small to reproduce the experimental modulations in both the two- and three-pulse ESEEM experiments. Therefore, the matrix contributions can be unambiguously excluded as the main source of the experimentally observed echo envelope modulations.

While the exchangeable protons of the protein matrix are well accounted for with this procedure, the water molecules present in the X-ray structure are not necessarily in the same position and of the same number as in the frozen protein solution used for the EPR measurements. However, inspection of the X-ray data showed that the pigments are contained in a hydrophobic cavity and that the closest possible approach for non-coordinated water molecules is 10 Å, which corresponds to a negligible modulation depth.

The peridinin molecule Per614 itself has two hydroxyl groups in the external rings, which could be exchanged with deuterons and cause the observed modulation of the spin echo envelope. The hyperfine interaction tensors for these two protons were calculated at the B3LYP/EPRII-6-311G(d,p) level of theory and the corresponding ESEEM signal was simulated and is shown in Fig. S4 of the Supplementary data. The modulation depth of the simulated time trace is much smaller than the experimental modulation depth due to the very weak interaction of these exchangeable protons on the peridinin molecule with the spin density delocalised over the whole conjugated chain of the molecule.

3.3.2. Exchangeable protons of the water molecule HOH701 in the photoprotective site

For the simulation of the ^{2}H ESEEM data of Fig. 3, we sought to determine a set of spin Hamiltonian parameters that would reproduce the frequencies, relative amplitudes, and initial modulation depths of the experimental data. The dipolar and isotropic hyperfine interaction parameters were optimised starting from the values obtained by quantum mechanical calculations in order to correctly reproduce the modulation depths and the attenuation of the modulations at all four field positions and for both the two- and the three-pulse ESEEM experiments in the time and frequency domain. The Euler angles describing the orientation of the hyperfine tensor with respect to the molecular frame were not changed significantly from those derived from DFT calculations, since the absence of modulations at the Z^{-} field position, arising from the colinearity of one principal axis of the hyperfine tensor with the Z axis of the ZFS tensor, was correctly reproduced with the calculated Euler angles.

The proton hyperfine interaction parameters giving the best overall agreement with the experimental data are reported together with the computed values in Table 2. Fig. 3 shows the results of such constrained simulations. The simulations agree well with experiments and the optimised hyperfine coupling parameters differ only slightly from those of the DFT calculations.

The hyperfine interaction of the water proton closer to the peridinin molecule (H1 in Fig. 4) is considerably stronger with respect to that of the more distant water proton coordinated to His66 (H2); hence the observed modulations are mainly due to the former.

The analysis of the exchangeable protons in the environment of Per614 has shown that these protons are not responsible for the experimentally observed modulations. However, they are expected to contribute somewhat to the modulation depth observed in the experimental spectra. For this reason, the ESEEM contributions due to the matrix deuterium nuclei were added to the main ESEEM envelopes according to the product rule. The addition of the matrix proton contribution leads to a small increase in modulation depth and to a slower damping of the modulations in time. The agreement with experimental data does not improve significantly by taking the matrix proton contributions into account (Fig. S5, Supplementary data).

In addition to the simulations based on a particular orientation of the water molecule as obtained from the geometry optimisations, simulations considering a distribution of different orientations [95] of the H1 water proton on a cone were also performed, resulting in an even shallower modulation depth (data not shown). This result confirms that the water molecule assumes a specific orientation as indicated by the geometry optimisations rather than a distribution of different orientations.

4. Discussion

In the present work the ESEEM experiment coupled with ^{1}H/^{2}H isotope exchange has been applied for the first time to a triplet state system, with the purpose of studying the interaction of the peridinin triplet state with a water molecule (HOH701) positioned at the interface between Per614 and Chl601 in the PCP antenna complex. This investigation was prompted by previous studies, where this water molecule was proposed to act as a bridge in the TTET occurring between Chl601 and Per614 and to be integral part of the photoprotective site in PCP [33,37]. The ESEEM technique is applied to gather information about the geometry and electronic structure of the putative photoprotective site.

The ESEEM time traces obtained by envelope division of the experimental time traces collected for the deuterated and protonated samples contain modulations due to the exchangeable protons in the environment of the triplet state of peridinin. Based on the results of the ESEEM simulations for exchangeable protons in the environment of Per614 in the PCP complex, it can be safely assumed that the observed modulations are not due only to matrix deuterons, since, even supposing all exchangeable protons to be substituted by deuterium nuclei; the simulated modulations would be too shallow to reproduce the experimental data. A further indication of the fact that the experimentally observed modulations do not originate from distant matrix nuclei is the absence of modulations in the ESEEM time trace collected at the Z^{-} field position since it is highly unlikely that the majority of matrix protons would be characterised by a hyperfine tensor with one principal axis aligned with the ZFS Z axis of the peridinin triplet state. The modulations arising from the hyperfine interaction of the exchangeable protons on the peridinin molecule itself are also too shallow to reproduce the experimental ESEEM time trace, hence they can be excluded as the origin of the experimentally observed modulations of the spin echo envelope as well.

In order to determine the contribution of the water molecule HOH701 to the observed ESEEM, the simulation of the ESEEM data was combined with quantum mechanical calculations. Geometry optimisations using the X-ray structure as a starting point were performed to define the structure of the photoprotective site in the PCP antenna complex, comprehensive of the hydrogen atoms absent in the X-ray structure [1]. In particular, the geometry optimisations were aimed at defining the position and orientation of the water molecule, which requires an accurate quantum mechanical description. The resulting model structures were then used for a calculation of the hyperfine interaction tensors. DFT calculated hyperfine parameters were used as guidelines and starting points in the simulations of the experimental spectra, they were optimised to simultaneously simulate multiple orientation-selective ESEEM traces, considering two- and three pulse sequences as well as time and frequency domains.

Triplet-state ESEEM is accompanied by orientation–selection due to the large anisotropy of the electron–electron dipolar interaction, allowing a precise determination of the relative orientation of the hyperfine interaction tensor of the coupled nuclei and the ZFS tensor of the peridinin triplet state. The presence of orientation selection poses strict constraints on the simulations: the hyperfine couplings have to correctly reproduce the ESEEM at all the considered field values. Once a set of

hyperfine parameters correctly simulating the time and frequency domain data of two- and three-pulse ESEEM experiments at several magnetic field values has been found, it can be confidently concluded that the interaction is characterised by this set of parameters. In order to increase the degree of accuracy even further, the DFT calculations of the hyperfine couplings served as extra constraints for the simulation parameters.

The hyperfine interaction parameters derived from simulation do not differ significantly from the DFT values calculated for the optimised structure of the photoprotective site obtained by our ONIOM approach. The orientations of the hyperfine interaction tensors, as well as the relative magnitude of the principal values of the dipolar hyperfine interaction tensor of the two water protons, are preserved. The absolute values differ slightly; the dipolar hyperfine interaction components resulting from the optimisation procedure are about 20% greater than the initial parameters calculated at B3LYP/EPRII-6-311G(d,p) level, which is in line with the estimated accuracy of the calculation of these parameters for weakly coupled nuclei, which are not directly part of the paramagnetic system [96,97].

In conclusion, the results of the simulation of multiple ESEEM traces clearly demonstrate that the observed electron spin echo envelope modulations are due to the water molecule HOH701. The satisfactory simulation of the full set of ESEEM experimental data based on the hyperfine interaction parameters of a single deuteron belonging to the water molecule at the interface between Chl601–Per614 greatly strengthens the evidence that this water molecule is part of the photoprotective site. The parameters, directly or indirectly extracted from the simulations, provide detailed information on the structure of the photoprotective site together with precise and reliable information on the spin density distribution in the water molecule.

In the ONIOM optimised structure of the photoprotective site, HOH701 is coordinated to the chlorophyll's Mg ion and situated at the interface between Per614/Chl601, with one proton coordinated to the His66 residue and the other pointing towards the peridinin chain. The orientation of this water molecule is well defined, based on the theoretical evaluation of the directions of the dipolar hyperfine tensor axes for the water protons with respect to the ZFS tensor frame of the peridinin triplet state and confirmed by spectral simulation. The presence of a single orientation of the water molecule rather than a distribution of different orientations is also clearly demonstrated.

While orientation and distance information can be extracted from the dipolar contribution to the hyperfine interaction, the isotropic coupling is a measure of the delocalisation of unpaired electron wave functions. Both the computed and optimised hyperfine interaction parameters include a non-zero isotropic hyperfine interaction constant for the water proton H1, proving that the triplet state wave function, largely localised on the conjugated chain of the peridinin polyene, is extended onto the water molecule. This is confirmed by quantum mechanical calculations, resulting in a small but significant spin density on the oxygen atom of the water molecule.

These results are strongly suggestive of a direct involvement of the water molecule at the interface of the two pigment partners in the TTET, favouring the process by extending the overlap between the wavefunctions of chlorophyll and peridinin.

As demonstrated in early studies by Closs and co-workers TTET is subjected to the same parameters that govern electron transfer [19,20]. In the weak-coupling limit, the TTET process, like electron transfer, is a non-adiabatic process with a rate constant defined by the golden rule [98]:

$$k = \frac{2\pi}{\hbar}|V_{TT}|^2 FCWDS \tag{1}$$

where FCWDS stands for the Frank–Condon weighted density of states and V_{TT} is the electronic coupling between the donor (D) and acceptor (A) triplet states, defined as:

$$V_{TT} = \left\langle \psi^{D}_{LUMO}(1)\psi^{A}_{HOMO}(2)\left|\frac{e^2}{r_{12}}\right|\psi^{A}_{LUMO}(1)\psi^{D}_{HOMO}(2)\right\rangle. \tag{2}$$

The distance dependence of this term reflects the distance dependence of the corresponding overlap integrals. TTET involves an exchange of two electrons of different spin and energy and for this reason, while in electron transfer the rate is dependent on a single overlap integral, in TTET the rate depends on the product of two overlap integrals, and therefore the exponential decay of the TTET rate with the distance r_{12} is twice that of electron transfer [19]. This process is thus characterised by even stricter distance requirements, favouring the hypothesis of the positive effect produced by the presence of a bridge molecule extending the overlap between the donor's and acceptor's wavefunctions for efficient energy transfer. In addition to the analogies with the formalism of electron transfer, the experiments by Closs and co-workers [19,20] also revealed an exponential attenuation of TTET couplings with donor–acceptor separation consistent with the superexchange model originally developed by McConnell for electron transfer [99]. The superexchange mechanism allows for virtual population of the triplet state localised on the connector such that V_{TT} can be expressed in the form [99]:

$$V_{TT} \propto \frac{V_{DC}V_{CA}}{\Delta E_{DC}} \tag{3}$$

where V_{DC} is the electronic coupling between donor and connector, and V_{CA} between connector and acceptor and ΔE_{DC} is the energy gap between the triplet states localised on the connector and the donor.

Superexchange models have been extensively used to interpret the dependence of the electronic coupling on the intervening medium in electron transfer processes and can be straightforwardly extended to the TTET mechanism. Most investigations on electron transfer have focused on donor–acceptor redox centres that are covalently attached to variable-length bridges, allowing to systematically analyse superexchange coupling via states of the covalent bridges [21]. At the same time, electron transfer in organic glasses and transfer within and between proteins provide compelling support that coupling does not require an entirely covalent pathway between the donor and the acceptor. Solvent molecules have been implicated in controlling the electronic coupling in systems containing solvent-separated ion pairs and in rigidly linked donor–acceptor pairs, in favourable geometries to host solvent molecules [9,100–102]. A number of theoretical studies have examined the effect of structured water molecules on the electronic coupling, providing convincing evidence that water molecules located in the vicinity of donor and acceptor units can mediate the electronic coupling [7,8,12,15]. Several experimental studies have substantiated the theoretical work on superexchange through water molecules, both in proteins and model systems [9,11,13].

Donor-to-connector and connector-to-acceptor separations, relative orientations, distribution and nodal patterns of the electron/energy transfer active orbitals on the donor, acceptor, and bridging molecule all influence the magnitude of the solvent-mediated coupling. The combined spectroscopic-computational parameters derived from the analysis of ESEEM data, highlight triplet wave function delocalisation onto the water molecule and constrained orientation of this molecule between the chlorophyll and carotenoid TTET partners, providing ideal conditions for superexchange-mediated TTET.

Although considerable effort has been directed toward the development of accurate methods to estimate the TTET coupling [103–107], theoretical characterisation of this parameter is currently not as developed as for electron transfer couplings. In the specific case of the PCP complex, computational studies, based on different approaches, have

provided estimates of the electronic coupling matrix elements for all chlorophyll *a* and peridinin pairs. Damjanović et al. estimated that the largest exchange coupling involved the Chl601–Per613 pair [108], in contrast to the EPR spectroscopic evidence [17]. Prompted by our previous investigations on the PCP complex [17,33,35], a theoretical study has been published, where the effect of the water molecule coordinated to chlorophyll on the TTET coupling has also been considered [14]. A method in the ab initio framework, previously developed by the same authors [104], was employed for the calculation of the TTET electronic coupling between pigments in PCP. The Chl602–Per624 pair gave the largest coupling among the four peridinins contained in one pigment cluster, in agreement with EPR results [17], but the bridging water molecule was found to give a negative contribution to the coupling, which was attributed to an opposite phase of the water-mediated coupling with respect to the through-space coupling. In addition to that, the same water molecule was surprisingly found to increase the coupling between Chl602 and an another peridinin molecule, Per623, positioned on the other side of the chlorophyll ring and previously ruled out as quencher of the chlorophyll triplet state [17]. However, in a previous study on π–π stacking interactions between pigments in the PCP complex, the same water molecule, at the interface between Chl602 and Per624, was found to give a significant contribution to the intermolecular interaction energy between the two pigments [109], in agreement with our results.

The double exchange integral plays a key role in determining the rate constants of the TTET processes and their accurate prediction is an important issue. The lack of consensus on the estimate of the TTET couplings derives from the origin of this small electronic interaction involving the tails of the wavefunctions. These contributions become even more important when considering TTET as compared to electron transfer processes because of the dependence of the rate constant on a double exchange integral [19,20]. For this reason an accurate description of the frontier orbital involved, also considering superexchange contributions from bridging molecules in detail, is an absolute requirement.

5. Conclusions

The results of ESEEM experiments on the ^2H_2O-exchanged protein complex combined with state-of-the-art computational methods have allowed the characterisation of the photoprotective site in the PCP antenna complex, providing experimental evidence for involvement of a structured water molecule in the TTET from chlorophyll to peridinin.

The following conclusions on the geometry and electronic structure of the photoprotective site can be drawn:

- The ESEEM data has been found to be compatible with a precise structure of the photoprotective site in which an ordered water molecule is coordinated to the chlorophyll Mg ion and hydrogen-bonded to the nearby histidine residue, while the other water proton points toward the conjugated chain of peridinin.
- The isotropic hyperfine coupling on the water protons indicates that the peridinin triplet state wavefunction is extended onto the water molecule.

The present investigation contributes to the issue of water-mediated electron/energy transfer processes by showing for the first time experimental evidence that water can contribute to an increase in the TTET electronic coupling between the donor and acceptor triplet states via superexchange. The involvement of the water bridge in the TTET process, which in PCP occurs with unity efficiency, represents an example of great relevance and a model for forthcoming investigations on this issue.

This study constitutes a promising framework for calculations of the TTET coupling, which are currently underway, combining in-silico treatments with spectroscopic evidence. This procedure will employ the geometries and electronic structures validated by ESEEM experiments, including explicit water-mediated electronic coupling. Starting from the PCP antenna complex, it can be extended to the study of TTET in natural antenna complexes of higher structural complexity, for which potential bridging protein residues have already been identified in the X-ray structures [64,91]. In a more general perspective, identification of super-exchange mediators in TTET is an important issue since this process plays a key role in natural and artificial photosynthesis: elucidation of the details of the mechanisms is fundamental in designing systems that not only efficiently harvest light but likewise photoprotect the system from singlet oxygen formation.

Acknowledgements

Financial support from MIUR (PRIN2008 prot. 20088NTBKR_004), the University of Padova (Progetto Strategico 2008, HELIOS, prot. STPD08RCX) and the Cariparo Foundation (M_3PC project) is gratefully acknowledged.

Appendix A. Supplementary data

Supplementary data to this article can be found online at http://dx.doi.org/10.1016/j.bbabio.2013.07.005 and includes: Quantum chemistry results, EPR spectra and details on EPR spectral simulations, as well as the full reference 73.

References

[1] E. Hofmann, P.M. Wrench, F.P. Sharples, R. Hiller, W. Welte, K. Diederichs, Structural basis of light harvesting by carotenoids: peridinin–chlorophyll–protein from *Amphidinium carterae*, Science 272 (1996) 1788–1791.
[2] In: D.R. Ort, C.F. Yocum (Eds.), Oxygenic Photosynthesis: The Light Reactions, Kluwer Academic Publishers, Dordrecht, 1996.
[3] V. Balzani, A. Credi, M. Venturi, Photochemical conversion of solar energy, ChemSusChem 1 (2008) 26–58.
[4] D. Gust, T.A. Moore, A.L. Moore, Realizing artificial photosynthesis, Faraday Discuss. 155 (2012) 9–26.
[5] M.R. Wasielewski, Self-assembly strategies for integrating light harvesting and charge separation in artificial photosynthetic systems, Acc. Chem. Res. 42 (2009) 1910–1921.
[6] In: D.S. Bendall (Ed.), Protein Electron Transfer, Bios Scientific Publishers, Oxford, UK, 1996.
[7] K.V. Mikkelsen, L.K. Skov, H. Nar, O. Farver, Electron self-exchange in azurin: calculation of the superexchange electron tunneling rate, Proc. Natl. Acad. Sci. U.S.A. 90 (1993) 5443–5445.
[8] J. Lin, I.A. Balabin, D.N. Beratan, The nature of aqueous tunneling pathways between electron-transfer proteins, Science 310 (2005) 1311–1313.
[9] O.S. Wenger, B.S. Leigh, R.M. Villahermosa, H.B. Gray, J.R. Winkler, Electron tunneling through organic molecules in frozen glasses, Science 307 (2005) 99–102.
[10] A. Migliore, S. Corni, R. Di Felice, E. Molinari, Water effects on electron transfer in azurin dimers, J. Phys. Chem. B 110 (2006) 23796–23800.
[11] S. Chakrabarti, M.F.L. Parker, C.W. Morgan, C.E. Schafmeister, D.H. Waldeck, Experimental evidence for water mediated electron transfer through bis-amino acid donor–bridge–acceptor oligomers, J. Am. Chem. Soc. 131 (2009) 2044–2045.
[12] O. Miyashita, H.L. Axelrod, J.N. Onuchic, Different scenarios for inter-protein electron tunneling: the effect of water-mediated pathways, J. Biol. Phys. 28 (2002) 383–394.
[13] I.M.C. van Amsterdam, M. Ubbink, O. Einsle, A. Messerschmidt, A. Merli, D. Cavazzini, G.L. Rossi, G.W. Canters, Dramatic modulation of electron transfer in protein complexes by crosslinking, Nat. Struct. Biol. 9 (2001) 48–52.
[14] Z.-Q. You, C.-P. Hsu, Ab initio study on triplet excitation energy transfer in photosynthetic light-harvesting complexes, J. Phys. Chem. A 115 (2011) 4092–4100.
[15] C. Curutchet, A.A. Voityuk, Distance dependence of triplet energy transfer in water and organic solvents: a QM/MD study, J. Phys. Chem. C 116 (2012) 22179–22185.
[16] T. Mani, D.M. Niedzwiedski, S.A. Vinogradov, Generation of phosphorescent triplet states via photoinduced electron transfer: energy and electron transfer dynamics in Pt porphyrin-rhodamine B dyads, J. Phys. Chem. A 116 (2012) 3598–3610.
[17] M. Di Valentin, S. Ceola, E. Salvadori, G. Agostini, D. Carbonera, Identification by time-resolved EPR of the peridinins directly involved in chlorophyll triplet quenching in the peridinin–chlorophyll *a*–protein from *Amphidinium carterae*, Biochim. Biophys. Acta Bioenerg. 1777 (2008) 186–195.
[18] D.L. Dexter, A theory of sensitized luminescence in solids, J. Chem. Phys. 21 (1953) 836–850.
[19] G.L. Closs, P. Piotrowiak, J.M. MacInnis, G.R. Fleming, Determination of long distance intramolecular triplet energy transfer rates. A quantitative comparison with electron transfer, J. Am. Chem. Soc. 110 (1988) 2652–2653.
[20] G.L. Closs, M.D. Johnson, J.R. Miller, P. Piotrowiak, A connection between intramolecular long-range electron, hole and triplet energy transfer, J. Am. Chem. Soc. 110 (1989) 3751–3753.
[21] M. Bixon, J. Jortner, Electron transfer via bridges, J. Chem. Phys. 107 (1997) 5154–5170.

[22] S.B. Sachs, S.P. Dudek, R.P. Hsung, L.R. Sita, J.F. Smalley, M.D. Newton, S.W. Feldberg, C.E.D. Chidsey, Rates of interfacial electron transfer through π-conjugated spacers, J. Am. Chem. Soc. 119 (1997) 10563–10564.

[23] L. Flamigni, F. Barigelletti, N. Armaroli, B. Ventura, J.-P. Collin, J.-P. Sauvage, J.A.G. Williams, Triplet–triplet energy transfer between porphyrins linked via a ruthenium(II) bisterpyridine complex, Inorg. Chem. 38 (1999) 661–667.

[24] A. Harriman, A. Khatyr, R. Ziessel, A.C. Benniston, An unusually shallow distance-dependence for triplet-energy transfer, Angew. Chem. Int. Ed. 39 (2000) 4287–4290.

[25] B. Albinsson, M.P. Eng, K. Petterson, M.U. Winters, Electron and energy transfer in donor–acceptor systems with conjugated molecular bridges, Phys. Chem. Chem. Phys. 9 (2007) 5847–5864.

[26] B. Albinsson, J. Mårtensson, Excitation energy transfer in donor–bridge–acceptor systems, Phys. Chem. Chem. Phys. 12 (2010) 7338–7351.

[27] J. Vura-Weis, S.H. Abdelwahed, R. Shukla, R. Rathore, M.A. Ratner, M. Wasielewski, Crossover from single-step tunneling to multistep hopping for molecular triplet energy transfer, Science 328 (2010) 1547–1550.

[28] J.A. Bautista, R.G. Hiller, F.P. Sharples, D. Gosztola, M. Wasielewski, H.A. Frank, Singlet and triplet energy transfer in the peridinin–chlorophyll *a*–protein from *Amphidinium carterae*, J. Phys. Chem. A 103 (1999) 2267–2273.

[29] F.J. Kleima, E. Hofmann, B. Gobets, I.H.M. van Stokkum, R. van Grondelle, K. Diederichs, H. van Amerongen, Förster excitation energy transfer in peridinin–chlorophyll-*a*–protein, Biophys. J. 78 (2000) 344–353.

[30] T. Polívka, R.G. Hiller, H.A. Frank, Spectroscopy of the peridinin–chlorophyll-*a*–protein: insights into light-harvesting strategy of marine algae, Arch. Biochem. Biophys. 458 (2007) 111–120.

[31] M.T.A. Alexandre, D.C. Lührs, I.H.M. van Stokkum, R. Hiller, M.-L. Groot, J.T.M. Kennis, R. van Grondelle, Triplet state dynamics in peridinin–chlorophyll-*a*–protein: a new pathway of photoprotection in LHCs? Biophys. J. 93 (2007) 2118–2128.

[32] T. Schulte, S. Johanning, E. Hofmann, Structure and function of native and refolded peridinin–chlorophyll–proteins from dinoflagellates, Eur. J. Cell Biol. 89 (2010) 990–997.

[33] M. Di Valentin, S. Ceola, G. Agostini, G.M. Giacometti, A. Angerhofer, O. Crescenzi, V. Barone, D. Carbonera, Pulse ENDOR and density functional theory on the peridinin triplet state involved in the photo-protective mechanism in the peridinin–chlorophyll *a*–protein from *Amphidinium carterae*, Biochim. Biophys. Acta Bioenerg. 1777 (2008) 295–307.

[34] M. Di Valentin, G. Agostini, E. Salvadori, S. Ceola, G.M. Giacometti, R.G. Hiller, D. Carbonera, Triplet–triplet energy transfer in peridinin–chlorophyll *a*–protein reconstituted with Chl a and Chl d as revealed by optically detected magnetic resonance and pulse EPR: comparison with the native PCP complex from *Amphidinium carterae*, Biochim. Biophys. Acta Bioenerg. 1787 (2009) 168–175.

[35] M. Di Valentin, E. Salvadori, S. Ceola, D. Carbonera, Pulsed EPR and ENDOR on the peridinin triplet state involved in the photoprotective mechanism in peridinin–chlorophyll *a*–proteins, Appl. Magn. Reson. 37 (2010) 191–205.

[36] J. Niklas, T. Schulte, S. Prakash, M. van Gastel, E. Hofmann, W. Lubitz, Spin-density distribution of the carotenoid triplet state in the peridinin–chlorophyll–protein antenna. A Q-band pulse electron-nuclear double resonance and density functional theory study, J. Am. Chem. Soc. 129 (2007) 15442–15443.

[37] M. Di Valentin, C. Tait, E. Salvadori, S. Ceola, H. Scheer, R. Hiller, D. Carbonera, Conservation of spin-polarization during triplet–triplet energy transfer in reconstituted peridinin–chlorophyll *a*–proteins from *Amphidinium carterae*, J. Phys. Chem. B 115 (2011) 13371–13380.

[38] W.B. Mims, J.L. Davis, J. Peisach, The accessibility of type I Cu(II) centers in laccase, azurin, and stellacyanin to exchangeable hydrogen and ambient water, Biophys. J. 45 (1984) 755–766.

[39] J. Peisach, W.B. Mims, J.L. Davis, Water coordination by heme iron in metmyoglobin, J. Biol. Chem. 259 (1984) 2704–2706.

[40] S.A. Dikanov, A.V. Astashkin, Y.D. Tsvetkov, M.G. Goldfeld, A.G. Chetverikov, Detection of deuterium nuclei in the immediate surroundings of P700 centers of plant photosynthesis by electron spin echo modulation, FEBS Lett. 224 (1987) 75–78.

[41] J. McCracken, J. Peisach, D.M. Dooley, Cu(II) coordination chemistry of amine oxidases: pulsed EPR studies of histidine imidazole, water, and exogeneous ligand coordination, J. Am. Chem. Soc. 109 (1987) 4064–4072.

[42] S.S. Eaton, J. Dubach, K.M. More, G.R. Eaton, G. Thurman, D.R. Ambruso, Comparison of the electron spin echo envelope modulation (ESEEM) for human lactoferrin and transferrin complexes of copper(II) and vanadyl ion, J. Biol. Chem. 264 (1989) 4776–4781.

[43] A.P. Hansen, R.D. Britt, M.P. Klein, C.J. Bender, G.T. Babcock, ENDOR and ESEEM studies of cytochrome c oxidase: evidence for exchangeable protons at the CuA site, Biochemistry 32 (1993) 13718–13724.

[44] A. Pacheco, P. Basu, P. Borbat, A.M. Raitsimring, J.H. Enemark, Multifrequency ESEEM spectroscopy of sulfite oxidase in phosphate buffer: direct evidence for coordinated phosphate, Inorg. Chem. 35 (1996) 7001–7008.

[45] D.A. Force, D.W. Randall, R.D. Britt, Proximity of acetate, manganese, and exchangeable deuterons to tyrosine Yz in acetate-inhibited photosystem II membranes: implications for the direct involvement of Yz in water-splitting, Biochemistry 36 (1997) 12062–12070.

[46] B.A. Diner, D.A. Force, D.W. Randall, R.D. Britt, Hydrogen bonding, solvent exchange, and coupled proton and electron transfer in the oxidation and reduction of redox-active tyrosine Yz in Mn-depleted core complexes of photosystem II, Biochemistry 37 (1998) 17931–17943.

[47] P. Dorlet, M. Di Valentin, G.T. Babcock, J. McCracken, Interaction of Yz with its environment in acetate-treated photosystem II membranes and reaction center cores, J. Phys. Chem. B 102 (1998) 8239–8247.

[48] Y. Deligiannakis, M. Louloudi, N. Hadjiliadis, Electron spin echo envelope modulation (ESEEM) spectroscopy as a tool to investigate the coordination environment of metal centers, Coord. Chem. Rev. 204 (2000) 1–112.

[49] L. Florens, B. Schmidt, J. McCracken, S. Ferguson-Miller, Fast deuterium access to the buried magnesium/manganese site in cytochrome c oxidase, Biochemistry 40 (2001) 7491–7497.

[50] M. Vogt, S. Lahiri, C.G. Hoogstraten, R.D. Britt, V.J. DeRose, Coordination environment of a site-bound metal ion in the hammerhead ribozyme determined by ^{15}N and ^{2}H ESEEM spectroscopy, J. Am. Chem. Soc. 128 (2006) 16764–16770.

[51] K.A. Ahrling, M.C. Evans, J.H.A. Nugent, R.J. Ball, R.J. Pace, ESEEM studies of substrate water and small alcohol binding to the oxygen-evolving complex of photosystem II during functional turnover, Biochemistry 45 (2006) 7069–7082.

[52] R.B. Muthukumaran, P.K. Grzyska, R.P. Hausinger, J. McCracken, Probing the iron–substrate orientation for taurine/alpha-ketoglutarate dioxygenase using deuterium electron spin echo envelope modulation spectroscopy, Biochemistry 46 (2007) 5951–5959.

[53] V. Kofman, S.A. Dikanov, A. Haran, J. Libman, A. Shanzer, D. Goldfarb, The coordination of VO to hydroxamate binders as studied by orientation selective ESEEM spectroscopy, J. Am. Chem. Soc. 117 (1995) 383–391.

[54] J.M. Canfield, K. Warncke, Active site reactant center geometry in the Co(II)-product radical pair state of coenzyme B12-dependent ethanolamine deaminase determined by using orientation–selection electron spin-echo envelope modulation spectroscopy, J. Phys. Chem. B 109 (2005) 3053–3064.

[55] M.M. Dicus, A. Conlan, R. Nechushtai, P.A. Jennings, M.L. Paddock, R.D. Britt, S. Stoll, Binding of histidine in the $(Cys)_3(His)_1$-coordinated [2Fe–2S] cluster of human mitoNEET, J. Am. Chem. Soc. 132 (2010) 2037–2049.

[56] H.-L. Yu, D.J. Sloop, S.I. Weissman, T.-S. Lin, J.R. Norris, M.K. Bowman, Electron spin echo modulation of the photoexcited triplets of anthracene in p-terphenyl crystals, J. Phys. Chem. 86 (1982) 4287–4290.

[57] T.S. Lin, Electron spin echo spectroscopy of organic triplets, Chem. Rev. 84 (1984) 1–15.

[58] W.J. Buma, E.J.J. Groenen, J. Schmidt, R. de Beer, An electron spin-echo envelope modulation study of the lowest triplet state of pyridine-d_5: spin-density distribution and structure, J. Chem. Phys. 91 (1989) 6549–6566.

[59] K. Steck, T. Wacker, W. Welte, F.P. Sharples, R.G. Hiller, Crystallization and preliminary X-ray analysis of a peridinin–chlorophyll *a* protein from *Amphidinium carterae*, FEBS Lett. 268 (1990) 48–50.

[60] F.P. Sharples, P.M. Wrench, K. Ou, R.G. Hiller, Two distinct forms of the peridinin–chlorophyll *a*–protein from *Amphidinium carterae*, Biochim. Biophys. Acta 1276 (1996) 117–123.

[61] W.B. Mims, Elimination of the dead-time artifacts in electron spin-echo envelope spectra, J. Magn. Reson. 59 (1984) 291–306.

[62] S. Stoll, A. Schweiger, EasySpin, a comprehensive software package for spectral simulation and analysis in EPR, J. Magn. Reson. 178 (2006) 42–55.

[63] S. Stoll, R.D. Britt, General and efficient simulation of pulse EPR spectra, Phys. Chem. Chem. Phys. 11 (2009) 6614–6625.

[64] M. Di Valentin, F. Biasibetti, S. Ceola, D. Carbonera, Identification of the sites of chlorophyll triplet quenching in relation to the structure of LHC-II from higher plants, evidence from EPR spectroscopy, J. Phys. Chem. B 113 (2009) 13071–13078.

[65] D.T. Edmonds, S.D. Goren, A.L. Mackay, A.A.L. White, W.F. Sherman, The nuclear quadrupole resonance of ^{2}D and ^{17}O in Ice II, J. Magn. Reson. 23 (1976) 505–514.

[66] D.W. Randall, A. Gelasco, M.T. Caudle, V.L. Pecoraro, R.D. Britt, ESE-ENDOR and ESEEM characterization of water and methanol ligation to a dinuclear Mn(III) Mn(IV) complex, J. Am. Chem. Soc. 119 (1997) 4481–4491.

[67] D.A. Force, D.W. Randall, G.A. Lorigan, K.L. Clemens, R.D. Britt, ESEEM studies of alcohol binding to the manganese cluster of the oxygen evolving complex of photosystem II, J. Am. Chem. Soc. 120 (1998) 13321–13333.

[68] P. Hohenberg, W. Kohn, Inhomogeneous electron gas, Phys. Rev. 136 (1964) B864–B871.

[69] W. Kohn, L.J. Sham, Self-consistent equations including exchange and correlation effects, Phys. Rev. 140 (1965) A1133–A1138.

[70] R.G. Parr, W. Yang, Density-functional theory of atoms and molecules, Oxford University Press, New York, 1989.

[71] S. Dapprich, I. Komáromi, S. Byun, K. Morokuma, M.J. Frisch, A new ONIOM implementation in Gaussian 98. 1. The calculation of energies, gradients and vibrational frequencies and electric field derivatives, J. Mol. Struct. (THEOCHEM) 462 (1999) 1–21.

[72] T. Vreven, S. Byun, I. Komáromi, S. Dapprich, J.A.J. Montgomery, K. Morokuma, M.J. Frisch, Combining quantum mechanics methods with molecular mechanics methods in ONIOM, J. Chem. Theory Comput. 2 (2006) 815–826.

[73] (a) M.J. Frisch, et al., Gaussian 03, Revision D.02, Gaussian, Inc., Wallingford, CT, 2004.;
(b) M.J. Frisch, et al., Gaussian 09, Revision B.01, Gaussian, Inc., Wallingford, CT, 2009.

[74] A.D. Becke, Density-functional thermochemistry. III. The role of exact exchange, J. Chem. Phys. 98 (1993) 5648–5652.

[75] C. Lee, W. Yang, R.G. Parr, Development of the Colle–Salvetti correlation-energy formula into a functional of the electron density, Phys. Rev. B 37 (1988) 785–789.

[76] J.P. Perdew, K. Burke, M. Ernzerhof, Generalized gradient approximation made simple, Phys. Rev. Lett. 77 (1996) 3865–3868.

[77] J.P. Perdew, M. Ernzerhof, K. Burke, Rationale for mixing exact exchange with density functional approximations, J. Chem. Phys. 105 (1996) 9982–9985.

[78] C. Adamo, V. Barone, Toward reliable density functional methods without adjustable parameters: the PBE0 model, J. Chem. Phys. 110 (1999) 6158–6169.

[79] L. Orian, S. Carlotto, M. Di Valentin, A. Polimeno, Charge transfer in model bioinspired carotene–porphyrin dyads, J. Phys. Chem. A 116 (2012) 3926–3933.

[80] A.K. Rappé, C.J. Casewit, K.S. Colwell, W.A.I. Goddard, W.M. Skiff, UFF, a full periodic-table force-field for molecular mechanics and molecular-dynamics simulations, J. Am. Chem. Soc. 114 (1992) 10024–10035.
[81] V. Barone, Characterization of the potential-energy surface of the HO_2 molecular-system by a density-functional approach, J. Chem. Phys. 101 (1994) 10666–10676.
[82] V. Barone, Inclusion of Hartree–Fock exchange in density-functional methods — hyperfine-structure of 2nd row atoms and hydrides, J. Chem. Phys. 101 (1994) 6834–6838.
[83] V. Barone, in: D.P. Chong (Ed.), Recent Advances in Density Functional Methods, Part I, World Scientific Publ. Co., Singapore, 1996.
[84] A.D. McLean, G.S. Chandler, Contracted Gaussian-basis sets for molecular calculations. 1. 2nd row atoms, Z = 11–18, J. Chem. Phys. 72 (1980) 5639–5648.
[85] K. Raghavachari, J.S. Binkley, R. Seeger, J.A. Pople, Self-consistent molecular orbital methods. 20. Basis set for correlated wave-functions, J. Chem. Phys. 72 (1980) 650–654.
[86] S. Kossmann, B. Kirchner, F. Neese, Performance of modern density functional theory for the prediction of hyperfine structure: meta-GGA and double hybrid functionals, Mol. Phys. 105 (2007) 2049–2071.
[87] F. Neese, Prediction of molecular properties and molecular spectroscopy with density functional theory: from fundamental theory to exchange-coupling, Coord. Chem. Rev. 253 (2009) 526–563.
[88] J. Tomasi, B. Mennucci, R. Cammi, Quantum mechanical continuum solvation models, Chem. Rev. 105 (2005) 2999–3093.
[89] V.I. Novoderezhkin, M.A. Palacios, H. van Amerongen, R. van Grondelle, Excitation dynamics in the LHCII complex of higher plants: modeling based on the 2.72 Angstrom crystal structure, J. Phys. Chem. B 109 (2005) 10493–10504.
[90] G. Zucchelli, D. Brogioli, A.P. Casazza, F.M. Garlaschi, R.C. Jennings, Chlorophyll ring deformation modulates Q(y) electronic energy in chlorophyll–protein complexes and generates spectral forms, Biophys. J. 93 (2007) 2240–2254.
[91] E. Salvadori, M. Di Valentin, C.M.W. Kay, A. Pedone, V. Barone, D. Carbonera, The electronic structure of the lutein triplet state in plant light-harvesting complex II, Phys. Chem. Chem. Phys. 14 (2012) 12238–12251.
[92] S.A. Dikanov, Y.D. Tsvetkov, Electron Spin Echo Envelope Modulation (ESEEM) Spectroscopy, CRC Press, Boca Raton, Florida, 1992.
[93] C.W. Bock, A. Kaufman, J.P. Glusker, Coordination of water to magnesium cations, Inorg. Chem. 33 (1994) 419–427.
[94] L. Kevan, M.K. Bowman, P.A. Narayana, R.K. Boeckman, V.F. Yudanov, Y.D. Tsvetkov, Electron spin echo envelope modulation of trapped radicals in disordered glassy systems: application to the molecular structure around excess electrons in γ-irradiated 2-methyltetrahydrofuran glass, J. Chem. Phys. 63 (1975) 409–416.
[95] K. Warncke, J. McCracken, Analysis of static distributions in hydrogen hyperfine interactions in randomly oriented radicals in the solid state by using ^{2}H electron spin echo envelope modulation spectroscopy: conformational dispersion of β-^{2}H coupling in the model tyrosyl radical, J. Chem. Phys. 103 (1995) 6829–6840.
[96] R. Improta, V. Barone, Interplay of electronic, environmental, and vibrational effects in determining the hyperfine coupling constants of organic free radicals, Chem. Rev. 104 (2004) 1231–1253.
[97] S. Kababya, J. Nelson, C. Calle, F. Neese, D. Goldfarb, Electronic structure of binuclear mixed valence copper azacryptates derived from integrated advanced EPR and DFT calculations, J. Am. Chem. Soc. 128 (2006) 2017–2029.
[98] R.A. Marcus, Chemical and electrochemical electron-transfer theory, Annu. Rev. Phys. Chem. 15 (1964) 155–196.
[99] H.M. McConnell, Intramolecular charge transfer in aromatic free radicals, J. Chem. Phys. 35 (1961) 508–515.
[100] A.S. Lukas, P.J. Bushard, M. Wasielewski, Electron transfer involving nonbonded superexchange interactions in rigid donor–acceptor arrays, J. Phys. Chem. A 106 (2002) 2074–2082.
[101] R. Kaplan, A.M. Napper, D.H. Waldeck, M.B. Zimmt, The role played by orbital energetics in solvent mediated electronic coupling, J. Phys. Chem. A 106 (2002) 1917–1925.
[102] M.B. Zimmt, D.H. Waldeck, Exposing solvent's roles in electron transfer reactions: tunneling pathway and solvation, J. Phys. Chem. A 107 (2003) 3580–3597.
[103] Z.-Q. You, C.-P. Hsu, G.R. Fleming, Triplet–triplet energy-transfer coupling: theory and calculation, J. Chem. Phys. 124 (2006) 044506.
[104] Z.-Q. You, C.-P. Hsu, The fragment spin difference scheme for triplet–triplet energy transfer coupling, J. Chem. Phys. 133 (2010) 074105.
[105] C.-P. Hsu, The electronic couplings in electron transfer and excitation energy transfer, Acc. Chem. Res. 42 (2008) 509–518.
[106] S. Yeganeh, T. Van Voorhis, Triplet excitation energy transfer with constrained density functional theory, J. Phys. Chem. C 114 (2010) 20756–20763.
[107] J.E. Subotnik, J. Vura-Weis, A.J. Sodt, M.A. Ratner, Predicting accurate electronic excitation transfer rates via Marcus theory with Boys or Edmiston–Ruedenberg localized diabatization, J. Phys. Chem. A 114 (2010) 8665–8675.
[108] A. Damjanović, T. Ritz, K. Schulten, Excitation transfer in the peridinin–chlorophyll–protein of *Amphidinium carterae*, Biophys. J. 79 (2000) 1695–1705.
[109] L. Mao, Y. Wang, X. Hu, π–π Stacking interactions in the peridinin–chlorophyll–protein of *Amphidinium carterae*, J. Phys. Chem. B 107 (2003) 3963–3971.